



LAWRENCE  
LIVERMORE  
NATIONAL  
LABORATORY

# Effects of pressure on the structure and lattice dynamics of $\alpha$ -glycine: A combined experimental and theoretical study

J. K. Hinton, S. Clarke, B. Steele, I. W. Kuo, N. Goldman, J. M. Zaug, E. Greenberg, V. B. Prakapenka, M. Kunz, M. P. Kroonblawd, E. Stavrou

December 6, 2018

CrystEngComm

## **Disclaimer**

---

This document was prepared as an account of work sponsored by an agency of the United States government. Neither the United States government nor Lawrence Livermore National Security, LLC, nor any of their employees makes any warranty, expressed or implied, or assumes any legal liability or responsibility for the accuracy, completeness, or usefulness of any information, apparatus, product, or process disclosed, or represents that its use would not infringe privately owned rights. Reference herein to any specific commercial product, process, or service by trade name, trademark, manufacturer, or otherwise does not necessarily constitute or imply its endorsement, recommendation, or favoring by the United States government or Lawrence Livermore National Security, LLC. The views and opinions of authors expressed herein do not necessarily state or reflect those of the United States government or Lawrence Livermore National Security, LLC, and shall not be used for advertising or product endorsement purposes.

# Effects of pressure on the structure and lattice dynamics of $\alpha$ -glycine: A combined experimental and theoretical study<sup>†</sup>

Jasmine K. Hinton,<sup>ab‡</sup> Samantha M. Clarke,<sup>a‡</sup> Brad A. Steele,<sup>a‡</sup> I-Feng W. Kuo,<sup>a</sup> Eran Greenberg,<sup>c</sup> Vitali B. Prakapenka,<sup>c</sup> Martin Kunz,<sup>d</sup> Matthew P. Kroonblawd,<sup>\*a</sup> Elissaios Stavrou<sup>\*a</sup>

Received Date

Accepted Date

DOI: 10.1039/xxxxxxxxxx

www.rsc.org/journalname

$\alpha$ -glycine is studied up to 50 GPa using synchrotron angle-dispersive X-ray powder diffraction (XRD), Raman spectroscopy, and quantum chemistry calculations performed at multiples levels of theory. Results from both XRD and Raman experiments reveal an extended pressure stability of the  $\alpha$  phase up to 50 GPa and the room temperature (RT) equation of state (EOS) was determined up to this pressure. This extended stability is corroborated by density functional theory (DFT) based calculations using the USPEX evolutionary structural search algorithm. Two calculated EOSs, as determined by DFT at  $T = 0$  K and semiempirical density functional tight-binding (DFTB) at RT, and the calculated Raman modes frequencies show a good agreement with the corresponding experimental results. Our work provides a definitive phase diagram and EOS for  $\alpha$ -glycine up to 50 GPa, which informs prebiotic synthesis scenarios that can involve pressures well in excess of 10 GPa.

## 1 Introduction

Glycine, the simplest amino acid, has attracted considerable attention that stems from its practical application in pharmaceuticals and as a model for understanding the formation of complex biomolecules necessary for the origins of life.<sup>1–8</sup> High pressures can substantially alter intermolecular interactions of organic molecules resulting in pressure-induced structural changes and chemical reactions including poly- and oligomerization.<sup>2,3,5,7,9,10</sup> For instance, extreme conditions realized during cometary or meteor impacts are thought to facilitate the chemistry needed to produce polypeptides and other biologically relevant molecules from simple precursors.<sup>7,11,12</sup> Understanding the room temperature structural behavior and equation of state (EOS) for glycine under static compression is a critical step for clarifying the role of

elevated thermodynamic conditions on the possible formation of polypeptides.

Pure glycine forms molecular crystals that exhibit rich polymorphism with three phases, stable at ambient conditions, identified to date.<sup>13</sup> Albrecht and Corey first determined its crystal structure in 1939, identifying the polymorph  $\alpha$ -glycine.<sup>14</sup> Later studies identified other polymorphs including the stable at ambient pressure  $\beta$ <sup>15</sup> and  $\gamma$ <sup>16</sup> phases and the high-pressure  $\delta$  phase.<sup>17</sup> Boldyreva *et al.* showed that  $\gamma$ -glycine is the most thermodynamically stable phase at ambient pressure through calorimetry measurements, while  $\alpha$ -glycine is metastable.<sup>13</sup> Glycine is also a known constituent of more complicated molecular systems such as glycine dihydrate, the structure of which was recently solved and proposed as the form of the glycine-water material found on NASA's Stardust mission.<sup>18</sup>

Despite the thermodynamic stability of the  $\gamma$  phase, it is substantially more difficult to grow crystals of  $\gamma$ -glycine compared to  $\alpha$ -glycine.<sup>13</sup> Most previous high-pressure studies focused on  $\alpha$ -glycine owing to difficulties in producing  $\gamma$ -glycine and the corresponding abundance and ease of obtaining samples of  $\alpha$ -glycine. At ambient conditions,  $\alpha$ -glycine crystallizes in a monoclinic  $P2_1/n$  crystal structure (SG 14,  $Z = 4$ ), see Fig. 1. This structure is characterized by the formation of a two-dimensional intermolecular hydrogen bonding network that lies within the  $a - c$  crystal plane.<sup>14</sup> In contrast, intermolecular binding along the  $b$  axis is limited to comparatively weaker van der Waals interactions.

<sup>a</sup> Lawrence Livermore National Laboratory, Physical and Life Sciences Directorate, P.O. Box 808, Livermore, CA 94550, USA E-mail: kroonblawd1@llnl.gov, stavrou1@llnl.gov

<sup>b</sup> University of Nevada, Las Vegas, Department of Physics and Astronomy, Las Vegas, NV, 89154, USA

<sup>c</sup> Center for Advanced Radiation Sources, University of Chicago, Chicago, IL 60637, USA.

<sup>d</sup> Advanced Light Source, Lawrence Berkeley National Laboratory, Berkeley, CA 94720, USA

<sup>†</sup> Electronic Supplementary Information (ESI) available: Pressure-dependent lattice parameters of  $\alpha$ -glycine, experimental and calculated Raman spectrum of  $\alpha$ -glycine at ambient conditions and calculated Raman spectra of  $\alpha$ -glycine at selected pressures. See DOI: 10.1039/b000000x/

<sup>‡</sup> These authors contributed equally to this work

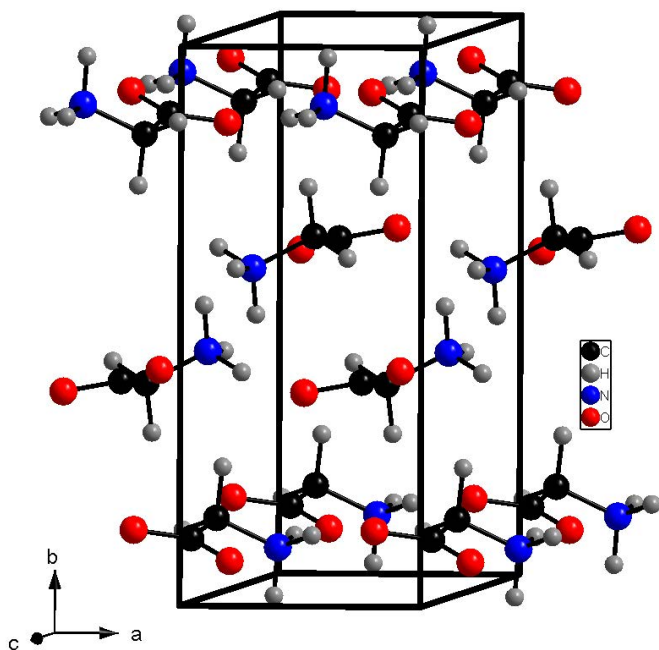


**Fig. 1** Schematic representation of the unit cell of  $\alpha$ -glycine at ambient temperature and pressure. Note that the unit cell contains four molecules and that additional molecules are rendered to highlight the packing structure. Atom colors are black, blue, red, and white for carbon, nitrogen, oxygen, and hydrogen, respectively

Previous structural studies<sup>10,17</sup> of  $\alpha$ -glycine based on X-ray and neutron diffraction do not report any phase transitions for  $\alpha$ -glycine up to at least 8.7 GPa. Murli *et al.*<sup>19</sup> performed a Raman spectroscopy study of  $\alpha$ -glycine up to 23 GPa and similarly report no evidence for a structural phase transition. However, Murli *et al.* do report subtle spectroscopic changes, including a broadening of the Raman modes at about 13 GPa, which can be attributed to the changes in the nature of hydrogen bonding or to the solidification of their pressure transmitting medium.<sup>20</sup> Although previous studies provided detailed information on  $\alpha$ -glycine at moderately high pressures, the maximum pressures reached are relatively small compared to the regimes that are readily accessible using a modern diamond anvil cell (DAC). Moreover, relevant prebiotic synthesis scenarios involve pressures well in excess of 10 GPa<sup>7,11,12</sup>.

Here we substantially extend previous structural studies of  $\alpha$ -glycine by conducting a combined experimental and theoretical investigation up to 50 GPa. Synchrotron angle-dispersive powder X-ray diffraction (PXRD) experiments and Raman spectroscopy measurements are coupled with quantum-based EOS calculations and a structure search using the evolutionary structural search algorithm, USPEX<sup>21-23</sup>. Surprisingly, and in contrast to the cases of  $\beta$ -<sup>24</sup> and  $\gamma$ -glycine<sup>17</sup>, we find that the ambient crystal structure of  $\alpha$ -glycine has an extensive pressure resilience and stability up to at least 50 GPa. The experimentally determined EOS was compared with calculated EOSs, as determined by density functional theory (DFT) at  $T = 0$  K and semiempirical density functional tight-binding (DFTB) at room temperature (RT), aiming to benchmark the two theoretical approaches.

## 2 METHODS

### 2.1 Experimental Methods

High purity, commercially available glycine (Sigma-Aldrich, >99.9% purity) was used for all experiments in this study. The crystal structure of the specimen provided by Sigma-Aldrich was characterized using Raman spectroscopy and PXRD at ambient conditions. Both techniques revealed that the specimen in hand had the crystal structure of  $\alpha$ -glycine (see Table 2 and Fig. S1 in ESI). Single crystals of  $\alpha$ -glycine were ground to a fine powder for angle-dispersive PXRD measurements and were loaded into a diamond anvil cell (DAC) with helium (He) as a pressure transmitting medium (PTM). Raman measurements were performed with small chips from the same batch of single crystals, with He or argon (Ar) as a PTM. Small quantities of ruby and gold powder were loaded to determine the pressure through ruby luminescence<sup>25</sup> and gold EOS<sup>26</sup>, respectively.

A Pilatus 1M CdTe detector was used at the undulator X-ray diffraction (XRD) Beamline 13-ID-D at GeoSoilEnviroCARS, sector13, APS, Chicago and a MAR-CCD detector was used at the Advanced Light Source, Lawrence Berkeley National Laboratory Beamline 12.2.2 to collect pressure-dependent X-ray diffraction data. The X-ray probing beam spot size was focused to approximately 2-4  $\mu\text{m}$  at GeoSoilEnviroCARS and to 10  $\mu\text{m}$  at beamline 12.2.2 using Kirkpatrick-Baez mirrors. Additional details on the XRD experimental setups are given in Prakapenka *et al.*<sup>27</sup> and Kunz *et al.*<sup>28</sup> Integration of powder diffraction patterns to yield scattering intensity versus  $2\theta$  diagrams and initial analysis were performed using the DIOPTAS program.<sup>29</sup> Calculated XRD patterns were produced using the POWDER CELL program<sup>30</sup> for the corresponding crystal structures and assuming continuous Debye rings of uniform intensity. Rietveld and Le Bail refinements were performed using the GSAS II<sup>31</sup> software. Indexing of XRD patterns was performed using the DICVOL program<sup>32</sup> as implemented in the FullProf Suite.

Raman measurements were performed using the 514.5 nm line of an Ar ion laser for excitation in the backscattering geometry. The laser probe diameter was approximately 2  $\mu\text{m}$ . Raman spectra were collected with a spectral resolution of 2  $\text{cm}^{-1}$  using a single-stage grating spectrograph equipped with a liquid nitrogen-cooled CCD array detector. Ultra-low frequency bandwidth solid-state notch filters allowed us to measure Raman spectra to within 10  $\text{cm}^{-1}$  of the Rayleigh line<sup>33</sup>. Thus, in contrast to previous Raman studies<sup>19</sup>, we were able to probe the low frequency lattice modes of  $\alpha$ -glycine inside the DAC, even at ambient conditions.

### 2.2 Computational Methods

#### 2.2.1 Equation of State

The lattice parameters and EOS for  $\alpha$ -glycine were obtained from quantum-based atomistic calculations performed at two levels of theory. First principles calculations were performed using density functional theory<sup>34,35</sup> (DFT) to obtain optimized ( $T = 0$  K) lattice parameters and atomic configurations for  $\alpha$ -glycine under hydrostatic compression. Semiempirical density functional tight-binding<sup>36-38</sup> (DFTB) calculations and molecular dynamics (MD)

simulations were used to independently obtain optimized lattice parameters and atomic configurations and also to gauge the magnitude of thermal contributions to the pressure. The efficiency of DFTB allows for quickly obtaining an estimate for the pressure under thermal conditions from MD. An alternative route would be to obtain an estimate for the thermal equilibrium lattice parameters using, for instance, the quasi-harmonic approximation<sup>39</sup>. All calculations were performed for an  $\alpha$ -glycine unit cell (40 atoms) using a three-dimensionally periodic simulation cell. In all cases, the electronic structure was evaluated without spin polarization.

DFT calculations were performed using the Vienna Ab-initio Simulation Package<sup>40</sup> (VASP) with the Perdew-Burke-Ernzerhof<sup>41</sup> (PBE) generalized gradient approximation functional with projector-augmented wave (PAW) potentials<sup>42,43</sup> and Grimme D2 dispersion corrections.<sup>44</sup> The wavefunction was calculated with a 700 eV plane wave energy cutoff and k-point density of  $0.05 \text{ \AA}^{-1}$ . The self-consistent field accuracy threshold was set to  $10^{-6}$  and optimizations of the ionic degrees of freedom were performed with a force-based accuracy threshold of  $1 \times 10^{-2} \text{ eV \AA}^{-1}$ . Optimized lattice parameters, atomic configurations, and hydrostatic pressure were obtained as a function of volumetric compression ratio  $V/V_0$  at  $T = 0 \text{ K}$ . The equilibrium volume  $V_0$  was calculated at ambient pressure and the volume was reduced sequentially in increments of  $0.02 \times V_0$ .

DFTB-level optimizations of the unit cell were performed using the DFTB+ code<sup>45</sup> and MD trajectories were integrated using extended Lagrangian Born-Oppenheimer dynamics<sup>46-49</sup> driven by LAMMPS<sup>50</sup> with forces and stresses evaluated by DFTB+. The DFTB parameter set used here was tuned to reproduce glycine condensation chemistry in aqueous solution. Specifically, we used the equal-weight variant of the force-matched DFTB model described in detail in Ref.<sup>8</sup> with additional universal force field dispersion corrections. Optimized cell lengths and angles were obtained for hydrostatic pressures in the interval  $0 \text{ GPa} \leq P \leq 50 \text{ GPa}$ . The optimizations were performed using a  $4 \times 4 \times 4$  Monkhorst-Pack<sup>51</sup> k-space mesh, Fermi-Dirac thermal smearing<sup>52</sup> with the electron temperature set to 25.85 meV (300 K), a self-consistent field accuracy threshold of  $2.7 \times 10^{-5} \text{ eV}$  ( $1 \times 10^{-6} \text{ au}$ ), and a force-based optimization threshold of  $5 \times 10^{-2} \text{ eV \AA}^{-1}$  ( $1 \times 10^{-3} \text{ au}$ ). The time step for the MD simulations was set to 0.2 fs and isochoric-isothermal (i.e., *NVT*) sampling was performed at 300 K with a Nosé-Hoover-style thermostat.<sup>53,54</sup> The electronic structure was evaluated during the MD simulations using a  $1 \times 1 \times 1$  Monkhorst-Pack<sup>51</sup> k-space mesh, four self-consistent charge cycles per time step, and Fermi-Dirac thermal smearing with the electronic temperature set equal to the instantaneous ionic kinetic temperature. Pressures at RT were computed from the last 5 ps of 10 ps *NVT* trajectories.

### 2.2.2 Structure Search

A molecular crystal structure search for possible polymorphs of glycine was performed at 50 GPa using the first principles evolutionary crystal structure prediction method USPEX<sup>21-23</sup>. The enthalpies were calculated using the same DFT parameters for the USPEX search as for the EOS calculation described above, with exceptions noted specifically below. The search was performed with

4 formula units in the unit cell (i.e., four glycine molecules). Four formula units covers a large portion of the energy landscape and is the same number of formula units contained in the  $\alpha$ -glycine unit cell. The computational expense precluded using a larger system size, thus those space groups with more than four formula units were not covered by the search. The search was performed with a population size of 50 for ten generations. A plane-wave energy cutoff of 450 eV and k-point density of  $0.07 \text{ \AA}^{-1}$  were used during the search for computational efficiency. Final enthalpy differences between various structures were calculated using a larger plane wave cutoff of 700 eV with a k-point density of  $0.05 \text{ \AA}^{-1}$ . A plane-wave cutoff of 450 eV was found to be reasonably well-converged, with the calculations using the higher 700 eV cutoff yielding only modest changes in the computed enthalpy differences on the order of  $1 \text{ meV atom}^{-1}$ .

### 2.2.3 Raman Spectra Calculations

Vibrational spectra were computed at a DFT-level of theory using the frozen phonon method (at the  $\Gamma$  point only) for each volume increment in the EOS. With the frozen phonon method, one computes the dynamical matrix through finite displacements of atoms about an optimized configuration. Diagonalization of the dynamical matrix yields eigenvalues and vectors that correspond to the phonon vibrational frequencies and modes, which were used to calculate the off-resonant Raman intensities for each mode. Raman intensities were calculated using derivatives of atomic polarizabilities with respect to applied electric fields within a linear response framework.<sup>55,56</sup>

## 3 RESULTS AND DISCUSSION

### 3.1 Pressure-Dependent Structural Properties

Figure 2 shows integrated PXRD patterns at selected pressures up to 50 GPa. The evolution of the XRD data show no discontinuous changes, such as the appearance/disappearance of Bragg peaks, up to the highest pressure considered. Moreover, there is no indication of pressure-induced amorphization, such as abrupt broadening or decrease of the Bragg peaks intensities. Thus, we conclude that the  $\alpha$  phase of glycine remains stable up to 50 GPa.

From the PXRD data of  $\alpha$ -glycine, we obtained the lattice parameters and the cell volume of  $\alpha$ -glycine structures as a function of pressure. The experimental results are compared with the calculated values shown in Figures 3(a) and S1 for the lattice parameters and in Fig. 3(b) for the cell volume. The DFT calculations at 0 K agrees more closely with the experiments for lattice parameter  $c$  and angle  $\beta$ , whereas DFTB at RT is more closely aligned for  $a$  and  $b$ , see Fig. S1. Experiment and theory (DFTB at RT and DFT at 0 K) agree closely for the lattice parameters up to the highest pressure of this study. One important consideration is that the DFTB model was not parameterized against crystalline glycine, so DFT serves as a higher-level validation of this significantly more computationally efficient model. As can be clearly seen in Figures 3(a) and S1, the **b**-axis exhibits a much higher compressibility in comparison to the other axes. Given that the **b**-axis corresponds to the distance between the glycine layers, it is plausible to attribute the higher compressibility to the weak intermolecular bonding and the higher free volume between the glycine layers.

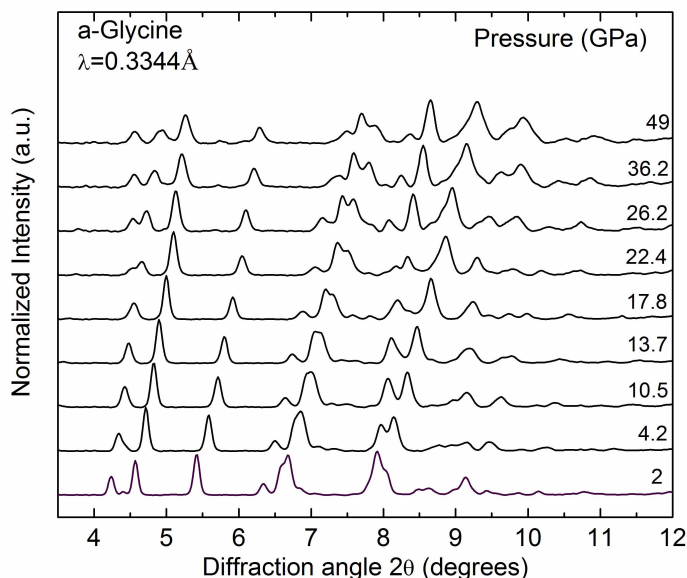


Fig. 2 PXRD patterns of  $\alpha$ -glycine at selected pressures.

We conducted EOS fits to the experimental and calculated  $P$ - $V$  data using a third-order Birch-Murnaghan EOS<sup>57</sup> and determined the bulk modulus  $B_0$  and the first derivative  $B'$ , see Table 1. The elastic parameters as determined from both the calculated EOSs imply a less compressible material compared with the experimental EOS, although at high pressures all EOSs become degenerate due to the higher  $B'$  value of the experimental EOS. The experimentally determined elastic parameters in this study are slightly different than the ones determined by Shinozaki *et al.*<sup>10</sup>, although from Fig. 3 one can see that the previous data points do lie close to the data points and to the EOS of this study. This can be attributed to the much larger pressure range in this study ( $\approx 50$  GPa vs 8 GPa) and also to the different type of EOSs used in the two studies.

**Table 1** Experimental and calculated elastic parameters of  $\alpha$ -glycine as determined in this study and from Shinozaki *et al.*<sup>10</sup>.

	$B$ (GPa)	$B'$	EOS Type
This study Exp.	14.8(20)	8.3(12)	3 <sup>rd</sup> order B-M
This study DFTB	19.7	6.2	3 <sup>rd</sup> order B-M
This study DFT	29.1	5.2	3 <sup>rd</sup> order B-M
Shinozaki <i>et al.</i>	19.5(7)	6.5(4)	Vinet

### 3.2 Pressure-Dependent Raman Scattering Properties

The Raman spectrum of the glycine specimen was determined at ambient conditions. Experimental Raman frequencies and mode assignments are listed in Table 2 and a comparison against a DFT-computed Raman spectrum is shown in Fig. S2. Both the Raman modes frequencies and the relative intensities are indicative of  $\alpha$ -glycine, see Table 2 in Ref. 58. The frequencies obtained here are in excellent agreement with previous studies.<sup>19,58–60</sup> However, we note that there are discrepancies with respect to the Raman mode assignments made in these reports. Following the previous high-

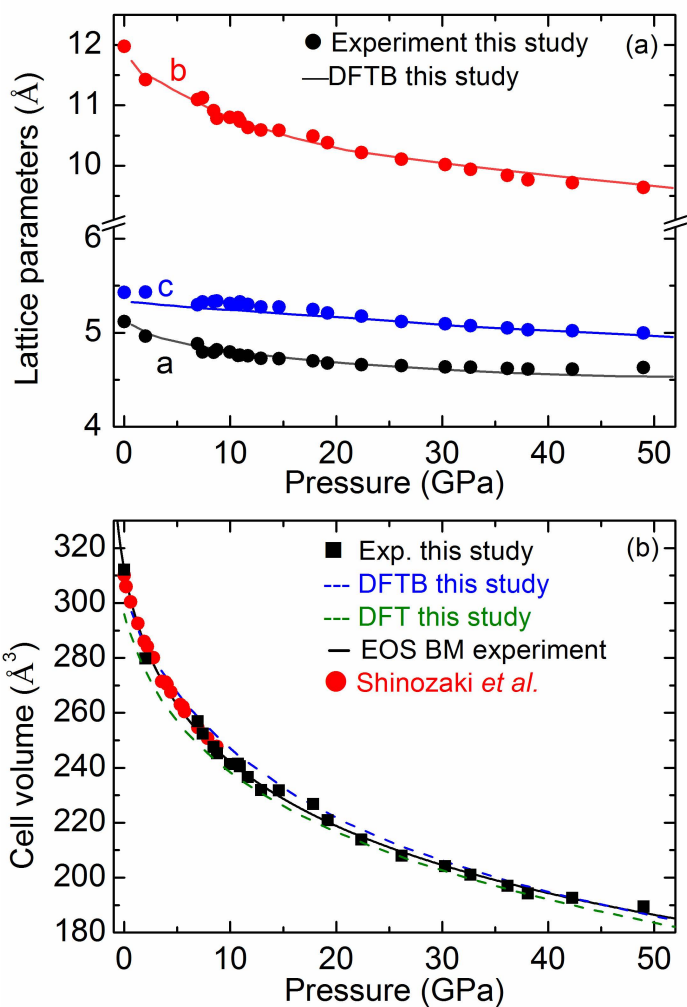


Fig. 3 (a) Pressure-dependent lattice parameters and (b) pressure-volume ( $P$ - $V$ ) data for  $\alpha$ -glycine. The solid line in (b) is the third-order Birch-Murnaghan EOS fit to the experimental data points<sup>57</sup>. Experimental values from Shinozaki *et al.*<sup>10</sup> are shown as red symbols.

pressure Raman study by Murli *et al.*,<sup>19</sup> we choose to adopt the mode assignments according to Machida *et al.*<sup>59</sup> as determined by intermolecular potential calculations.

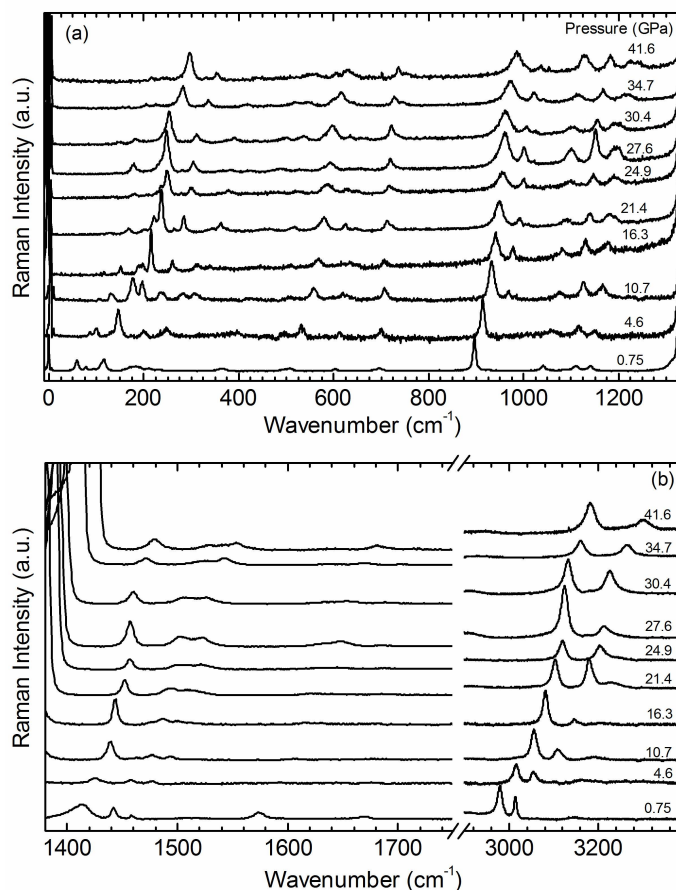
High pressure Raman measurements (see Figure 4) are in good overall agreement with the previous study by Murli *et al.* All but one ( $\text{NH}_3$  symmetric bending) Raman mode exhibit (typical) blue shifting with increasing pressure. We observe the appearance of additional Raman modes at  $\approx 5$  GPa, such as the splitting of the  $\text{CH}_2$  rocking modes. New Raman modes also appear at  $\approx 13$  GPa and at  $\approx 20$  GPa. Following the conclusions of Ref. 19, we attribute the appearance of these modes to the different frequency-pressure slopes of Raman modes with nearly degenerate frequencies at ambient conditions and/or an intensity enhancement due to changes in hydrogen bonding. We do not observe a prominent increase of the Raman mode widths above 13 GPa, presumably due to our use of a more hydrostatic pressure transmitting medium<sup>20</sup> compared to the study of Murli *et al.* Further studies, presumably a neutron diffraction study above 10 GPa, would be needed to clarify the origin and nature of changes to hydrogen

**Table 2** Comparison of Raman-active vibrational mode frequencies ( $\text{cm}^{-1}$ ) in  $\alpha$ -glycine as observed in this study and in previous studies<sup>58,59</sup>.

This Study	Ref. 58	Ref. 59	Assignment
52.4	52	52	Lattice mode
73.4	74	72	Lattice mode
87	-	-	Lattice mode
109	110	109	Lattice mode
164	163	157	Lattice mode
180	180	-	Lattice mode
197	198	194	CO <sub>2</sub> torsion
358	356	356	CCN deformation
492	491	495	NH <sub>3</sub> torsion
501	510	-	CO <sub>2</sub> rock
599	602	603	CO <sub>2</sub> wagging
694	694	695	CO <sub>2</sub> bending
893	894	890	C-C stretching
920	-	-	CH <sub>2</sub> rocking
1035	1035	1034	C-N stretching
1106	1108	-	NH <sub>3</sub> rocking
1137	1133	1139	NH <sub>3</sub> rocking
-	-	1324	CH <sub>2</sub> wagging
1410	1409	1410	CO <sub>2</sub> symm. stretching
1440	1446	1441	CH <sub>2</sub> bending
1454	-	-	CH <sub>2</sub> scissoring
1513	-	1513	NH <sub>3</sub> symmetric bending
1568	1574	1570	CO <sub>2</sub> asymm. stretching
-	-	1642	NH <sub>3</sub> asymm. bending
2825-2910	2976	-	Combination bands
2976	2973	-	CH <sub>2</sub> symm. stretching
3007	3008	-	CH <sub>2</sub> asymm. stretching
3143	3150	-	N-H stretching modes

bonding. No other pressure-induced spectroscopic discontinuities were observed above 23 GPa up to the highest pressure of this study (42 GPa). Most importantly, the number and relative intensity of the external lattice modes remains practically constant with increasing pressure. The fact that we observed no change of the frequency-pressure slope for the N-H stretching modes indicates the absence of a substantial change in intermolecular hydrogen bonding<sup>19</sup>. Thus, the results of Raman spectroscopy corroborate with our PXRD results, indicating an extensive pressure stability of  $\alpha$ -glycine up to 50 GPa.

Raman spectra computed with DFT agree closely with experiment except for a discrepancy in the N-H stretching modes. In particular, DFT and experiment display the same number of Raman-active modes and the same trend with pressure (see Figures S2 and S4). Two N-H stretching bands exist in the calculated spectra between 2700-2900  $\text{cm}^{-1}$  that are not observed in experiment. In addition, the calculated NH<sub>3</sub> torsional and symmetric bending modes have a different slope versus pressure compared to experiment, see Figure 5. The error in the frequency and intensity of these modes is likely due to the well-known inadequate description of electron correlation (and hence hydrogen bonding) at the PBE-D2 level of theory.<sup>61-68</sup> While Hartree-Fock based methods

**Fig. 4** Raman spectra of  $\alpha$ -glycine at selected pressures up to 42 GPa.

that explicitly include electron correlation such as Møller-Plesset (MP2), coupled clusters (CC), or configuration interaction (CI) would more accurately describe the hydrogen bonding, they are prohibitively expensive. Since the rest of the spectra shows relatively good agreement to experiment, we conclude the PBE-D2 level of theory is sufficiently accurate.

Both DFT and experiment show a convoluted N-H stretching band at high frequency near 3200  $\text{cm}^{-1}$ . DFT reveals a distinct high frequency N-H mode and two low frequency N-H bands. This splitting occurs because the DFT-optimized structure exhibits three distinct N-H...O separation distances leading to two relatively short N-H...O hydrogen bonds and one long hydrogen bond. (At 0 GPa, these three hydrogen bond lengths are 1.678 Å, 1.717 Å, and 1.937 Å.) The two shorter (stronger) hydrogen bonds cause the N-H bond to be longer and thus the frequency of N-H stretching mode to be smaller (2710 and 2875  $\text{cm}^{-1}$ ). In contrast, the longer hydrogen bond allows the N-H bond to be shorter, leading to a second stretching mode at higher frequency (3162  $\text{cm}^{-1}$ ). Calculated and experimental frequencies are in good agreement between 400-1800  $\text{cm}^{-1}$ . Modest differences in the frequencies are likely due to the fact that the calculated spectra correspond to 0 K. For instance, the splitting of CH<sub>2</sub> rocking modes near 5 GPa observed in experiment is clearly reproduced in the calculated spectra. The high frequency C-H stretching modes show relatively good agreement against experiment. There is a convolution of C-H stretching

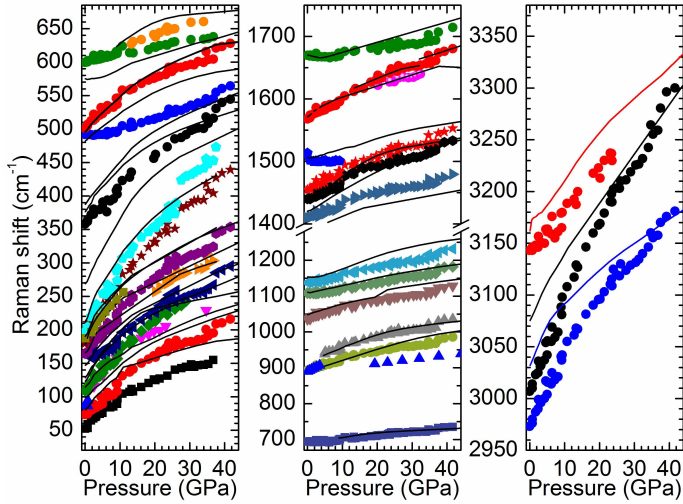


**Fig. 5** Raman mode frequencies of  $\alpha$ -glycine as a function of pressure. Experimental and calculated values are shown with solid symbols and solid curves, respectively.

modes in the calculated spectra that combine to form two main bands that follow the same trend with pressure as seen in the experimental spectra.

### 3.3 $F$ - $f$ finite-strain analysis

Both PXRD and Raman spectroscopy data clearly indicate the absence of a first order phase transition up to the highest pressure of this study. In order to further explore the possibility of a subtle structural modification we performed additional analysis of the XRPD results, including examining the pressure evolution of the normalized lattice parameters and also plotting the  $P$ - $V$  data using the  $F$ - $f$  finite-strain formalism<sup>69</sup>. That is, we plot the normalized stress  $F_E$ , as a function of Eulerian strain  $f_E$ . The  $F$ - $f$  EOS is ideal to probe subtle structural changes that relax built-up unit cell stress. Application of the  $F$ - $f$  EOS model reveals that the pressure-dependent stress exhibits a linear response to applied strain up to 50 GPa within the established errors (see Fig. 6(b)). Thus, there is no indication of a pressure- or strain-induced modification of the initial structure. Moreover, there is no prominent change of the compressibility (see Fig. 6(a)) of all axes up to 50 GPa. Consequently, we conclude there is an absence of even subtle structural modifications of  $\alpha$ -glycine.

### 3.4 USPEX Structure Search

Aiming to better understand the extensive pressure stability of the  $\alpha$ -glycine structure, we performed a structural search for alternative (meta)stable polymorphs of glycine at 50 GPa using the USPEX evolutionary structural search algorithm. Our main aim was to clarify whether the  $\alpha$  phase is the most thermodynamically stable phase of glycine at 50 GPa, or if there exist other lower enthalpy phases, as is the case at ambient pressure. One distinct possibility is that the  $\alpha$  phase may be metastable under pressure (similar to other systems<sup>70</sup>), which only persists in our experiments due to lack of sufficiently strong perturbations such as elevated temperatures.

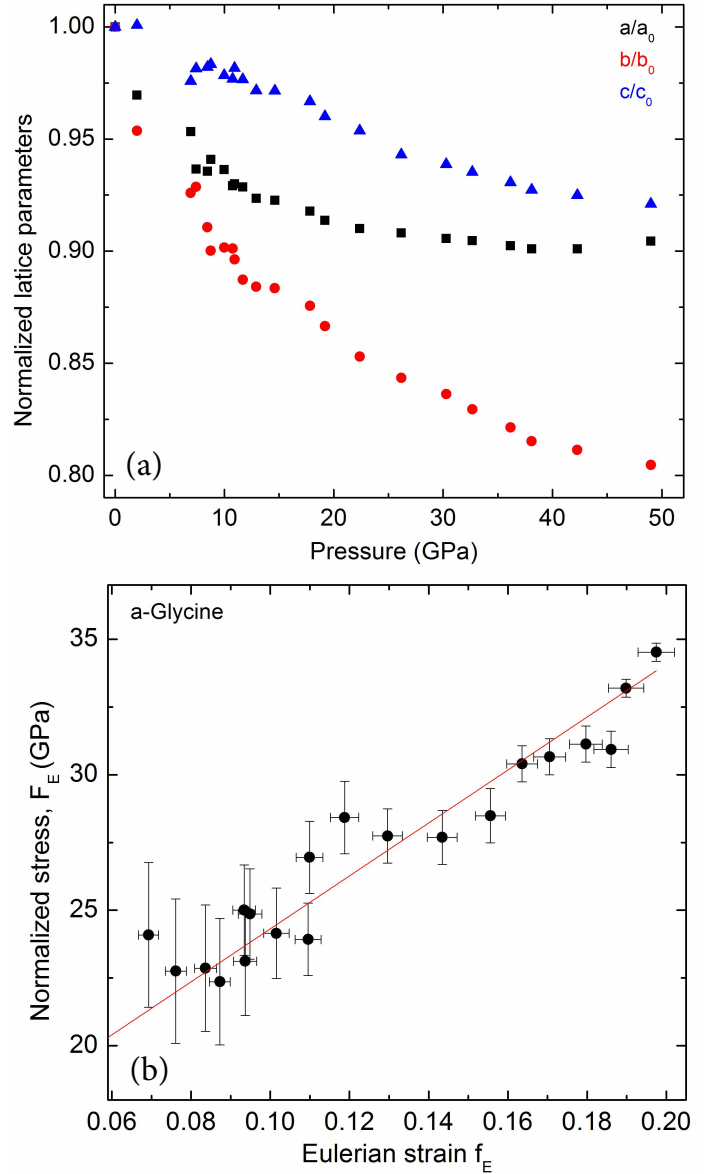


**Fig. 6** (a) Normalized lattice parameters and (b)  $F$ - $f$  EOS plot of the  $P$ - $V$  data. The red line is a linear fit to the  $F$ - $f$  data.

The USPEX search revealed several structures that were higher in enthalpy ( $\Delta H$ ) than  $\alpha$ -glycine with space groups  $P2_1/c$  and  $P2_12_12_1$ . We identified four unique structures within 40 meV atom<sup>-1</sup> of  $\alpha$ -glycine, which we list in Table 3. While similar in enthalpy, the structures exhibit different packing structures relative to the  $\alpha$  phase. The structure closest in enthalpy is 6 meV atom<sup>-1</sup> higher in enthalpy, see Table 3. The enthalpy of  $\beta$ -glycine and  $\gamma$ -glycine is 31 meV atom<sup>-1</sup> and 68 meV atom<sup>-1</sup> higher in enthalpy than  $\alpha$ -glycine at 50 GPa, respectively. The results of our USPEX calculations indicate that, although additional polymorphs are possible, the ones found are less thermodynamically favored.

## 4 Conclusions

The structural evolution of  $\alpha$ -glycine was explored by a combined experimental and computational study up to 50 GPa. A near perfect agreement is found between experimental and calculated

**Table 3** Enthalpy difference between  $\alpha$ -glycine and glycine polymorphs found during the structure search at 50 GPa. The polymorphs are characterized by their crystallographic space groups.

Space Group	$\Delta H$ (meV atom <sup>-1</sup> )
$P2_1/n$ ( $\alpha$ -glycine)	0
$P2_12_12_1$	6
$P2_1/c$	19
$P2_12_12_1$	19
$P2_1$ ( $\beta$ -glycine)	31
$P2_1/c$	38
$P3_2$ ( $\gamma$ -glycine)	68

equations of state, as determined in this study by two independent theoretical approaches (DFT at  $T = 0$  K and DFTB at room temperature). We conclude from the results of both experimental measurements (X-ray diffraction and Raman spectroscopy) and calculations performed at two levels of theory that no structural phase transition was observed up to 50 GPa. No subtle structural modifications were evident from an analysis of the normalized lattice parameters and the  $F - f$  finite-strain formalism. The stability of  $\alpha$ -glycine at 50 GPa was further corroborated by a crystal structure search using USPEX calculations. Our work provides a definitive phase diagram and EOS of  $\alpha$ -glycine, the most abundant polymorph of glycine, up to pressures that are relevant to prebiotic synthesis scenarios that involve pressures well in excess of 10 GPa. Moreover, our study provides a baseline for the evolution of simple aminoacid systems under pressure, by substantially exceeding the pressure range of the structural study of any previous glycine polymorph.

## Conflicts of interest

There are no conflicts to declare.

## Acknowledgments

This work was performed under the auspices of the U. S. Department of Energy by Lawrence Livermore National Security, LLC under Contract DE-AC52-07NA27344. We gratefully acknowledge the LLNL LDRD program for funding support of this project under 18-LW-036. Part of this work was performed at GeoSoilEnviroCARS (The University of Chicago, Sector 13), Advanced Photon Source (APS), Argonne National Laboratory. GeoSoilEnviroCARS is supported by the National Science Foundation - Earth Sciences (EAR-1634415) and Department of Energy-GeoSciences (DE-FG02-94ER14466). This research used resources of the Advanced Photon Source, a U.S. Department of Energy (DOE) Office of Science User Facility operated for the DOE Office of Science by Argonne National Laboratory under Contract No. DE-AC02-06CH11357. Use of the COMPRES-GSECARS gas loading system was supported by COMPRES under NSF Cooperative Agreement EAR -1606856 and by GSECARS through NSF grant EAR-1634415 and DOE grant DE-FG02-94ER14466. The ALS is supported by the Director, Office of Science, BES of DOE under Contract No. DE-AC02-05CH11231, DE-AC02-06CH11357. The authors thank Sergey N. Tkachev and Andrew Doran for helping with the gas

loading at sector 13 GSECARS (APS) and Beamline 12.2.2. (ALS) respectively. We thank J. M. Zaug and A. Salamat for fruitful discussions and for a critical reading of the manuscript.

## References

- H. Borsook, *Adv. Protein Chem.*, 1953, **8**, 127 – 174.
- E. L. Shock, *Geochim. Cosmochim. Acta*, 1992, **56**, 3481 – 3491.
- E.-i. Imai, H. Honda, K. Hatori, A. Brack and K. Matsuno, *Science*, 1999, **283**, 831 – 833.
- A. Brack, *Chem. Biodivers.*, 2007, **4**, 665 – 679.
- E. Schreiner, N. N. Nair and D. Marx, *J. Am. Chem. Soc.*, 2009, **131**, 13668 – 13675.
- G. Danger, R. Plasson and R. Pascal, *Chem. Soc. Rev.*, 2012, **41**, 5416 – 5429.
- H. Sugahara and K. Mimura, *Geochem. J.*, 2014, **48**, 51 – 62.
- M. P. Kroonblawd, F. Pietrucci, A. M. Saitta and N. Goldman, *Journal of Chemical Theory and Computation*, 2018, **14**, 2207–2218.
- C. Fujimoto, A. Shinozaki, K. Mimura, T. Nishida, H. Gotou, K. Komatsu and H. Kagi, *Chem. Commun.*, 2015, **51**, 13358–13361.
- A. Shinozaki, K. Komatsu, H. Kagi, C. Fujimoto, S. Machida, A. Sano-Furukawa and T. Hattori, *J. Chem. Phys.*, 2018, **148**, 044507.
- N. Goldman, E. J. Reed, L. E. Fried, I.-F. William Kuo and A. Maiti, *Nat. Chem.*, 2010, **2**, 949.
- Z. Martins, M. C. Price, N. Goldman, M. A. Sephton and M. J. Burchell, *Nat. Geosci.*, 2013, **6**, 1045.
- E. V. Boldyreva, V. A. Drebuschak, T. N. Drebuschak, I. E. Paukov, Y. A. Kovalevskaya and E. S. Shutova, *J. Therm. Anal. Calorim.*, 2003, **73**, 409–418.
- G. Albrecht and R. B. Corey, *J. Am. Chem. Soc.*, 1939, **61**, 1087–1103.
- Y. Iitaka, *Nature*, 1959, **183**, 390.
- Y. Iitaka, *Acta Crystallogr.*, 1961, **14**, 1–10.
- A. Dawson, D. R. Allan, S. A. Belmonte, S. J. Clark, W. I. F. David, P. A. McGregor, S. Parsons, C. R. Pulham and L. Sawyer, *Crystal Growth & Design*, 2005, **5**, 1415–1427.
- W. Xu, Q. Zhu and C. T. Hu, *Angew. Chem. Int. Ed.*, 2017, **56**, 2030–2034.
- C. Murli, S. M. Sharma, S. Karmakar and S. Sikka, *Physica B*, 2003, **339**, 23 – 30.
- S. Klotz, J.-C. Chervin, P. Munsch and G. L. Marchand, *J. Phys. D: Appl. Phys.*, 2009, **42**, 075413.

- 21 C. W. Glass, A. R. Oganov and N. Hansen, *Comp. Phys. Comm.*, 2006, **175**, 713–720.
- 22 A. O. Lyakhov, A. R. Oganov and M. Valle, *Comp. Phys. Comm.*, 2010, **181**, 1623–1632.
- 23 A. R. Oganov and C. W. Glass, *J. Chem. Phys.*, 2006, **124**, 244704.
- 24 E. V. Boldyreva, S. N. Ivashevskaya, H. Sowa, H. Ahsbahs and H.-P. Weber, *Dokl. Phys. Chem.*, 2004, **396**, 111–114.
- 25 K. Syassen, *High Pres. Res.*, 2008, **28**, 75.
- 26 M. Matsui, *International Conference On High Pressure Science and Technology, Joint AIRAPT-22 and HPCJ-50*, 2010, **215**, 012197.
- 27 V. B. Prakapenka, A. Kubo, A. Kuznetsov, A. Laskin, O. Shkurikhin, P. Dera, M. L. Rivers and S. R. Sutton, *High Pres. Res.*, 2008, **28**, 225–235.
- 28 M. Kunz, A. MacDowell, W. Caldwell, D. Cambie, R. Celestre, E. Domning, R. Duarte, A. Gleason, J. Glossinger, N. Kelez, D. Plate, T. Yu, J. Zaug, H. Padmore, R. Jeanloz, A. Alivisatos and S. Clark, *J. Synchrotron Radiat.*, 2005, **12**, 650.
- 29 C. Prescher and V. B. Prakapenka, *High Pres. Res.*, 2015, **35**, 223–230.
- 30 W. Kraus and G. Nolze, *J. Appl. Crystallogr.*, 1996, **29**, 301–303.
- 31 B. H. Toby and R. B. Von Dreele, *J. Appl. Crystallogr.*, 2013, **46**, 544–549.
- 32 A. Boultif and D. Louër, *J. Appl. Crystallogr.*, 2004, **37**, 724–731.
- 33 E. Stavrou, M. Ahart, M. F. Mahmood and A. F. Goncharov, *Sci. Rep.*, 2013, **3**, 1290–.
- 34 P. Hohenberg and W. Kohn, *Phys. Rev.*, 1964, **136**, B864–B871.
- 35 W. Kohn and L. J. Sham, *Phys. Rev.*, 1965, **140**, A1133 – A1138.
- 36 D. Porezag, T. Frauenheim, T. Köhler, G. Seifert and R. Kaschner, *Phys. Rev. B: Condens. Matter Mater. Phys.*, 1995, **51**, 12947 – 12957.
- 37 M. Elstner, D. Porezag, G. Jungnickel, J. Elsner, M. Haugk, T. Frauenheim, S. Suhai and G. Seifert, *Phys. Rev. B: Condens. Matter Mater. Phys.*, 1998, **58**, 7260 – 7268.
- 38 P. Koskinen and V. Mäkinen, *Comput. Mater. Sci.*, 2009, **47**, 237 – 253.
- 39 A. Erba, J. Maul and B. Civalleri, *Chem. Commun.*, 2016, **52**, 1820–1823.
- 40 G. Kresse and J. Furthmüller, *Comput. Mater. Sci.*, 1996, **6**, 15 – 50.
- 41 J. P. Perdew, K. Burke and M. Ernzerhof, *Phys. Rev. Lett.*, 1996, **77**, 3865 – 3868.
- 42 P. E. Blöchl, *Phys. Rev. B*, 1994, **50**, 17953–17979.
- 43 G. Kresse and D. Joubert, *Phys. Rev. B*, 1999, **59**, 1758–1775.
- 44 S. Grimme, *J. Comp. Chem.*, 2006, **27**, 1787–1799.
- 45 B. Aradi, B. Hourahine and T. Frauenheim, *J. Phys. Chem. A*, 2007, **111**, 5678 – 5684.
- 46 A. M. N. Niklasson, C. J. Tymczak and M. Challacombe, *Phys. Rev. Lett.*, 2006, **97**, 123001.
- 47 A. M. N. Niklasson, *Phys. Rev. Lett.*, 2008, **100**, 123004.
- 48 A. M. N. Niklasson, P. Steneteg, A. Odell, N. Bock, M. Challacombe, C. J. Tymczak, E. Holmström, G. Zheng and V. Weber, *J. Chem. Phys.*, 2009, **130**, 214109.
- 49 G. Zheng, A. M. N. Niklasson and M. Karplus, *J. Chem. Phys.*, 2011, **135**, 044122.
- 50 S. Plimpton, *J. Comput. Phys.*, 1995, **117**, 1 – 19.
- 51 H. J. Monkhorst and J. D. Pack, *Phys. Rev. B*, 1976, **13**, 5188–5192.
- 52 N. D. Mermin, *Phys. Rev.*, 1965, **137**, A1441–A1443.
- 53 S. Nosé, *J. Chem. Phys.*, 1984, **81**, 511 – 519.
- 54 W. G. Hoover, *Phys. Rev. A: At., Mol., Opt. Phys.*, 1985, **31**, 1695 – 1697.
- 55 M. Lazzeri and F. Mauri, *Phys. Rev. Lett.*, 2003, **90**, 036401.
- 56 D. Porezag and M. R. Pederson, *Phys. Rev. B*, 1996, **54**, 7830–7836.
- 57 F. Birch, *J. Geophys. Res.*, 1978, **83**, 1257–1268.
- 58 Y. Shi and L. Wang, *J. Phys. D: Appl. Phys.*, 2005, **38**, 3741.
- 59 K. Machida, A. Kagayama, Y. Saito, Y. Kuroda and T. Uno, *Spectrochimica Acta Part A: Molecular Spectroscopy*, 1977, **33**, 569 – 574.
- 60 H. Stenback, *J. Raman Spectrosc.*, 1976, **5**, 49–55.
- 61 J. E. D. Bene and M. J. Jordan, *Journal of Molecular Structure: THEOCHEM*, 2001, **573**, 11 – 23.
- 62 T. Steiner, *Angewandte Chemie International Edition*, 2002, **41**, 48–76.
- 63 T. M. Watson and J. D. Hirst, *The Journal of Physical Chemistry A*, 2002, **106**, 7858–7867.
- 64 J. Ireta, J. Neugebauer and M. Scheffler, *The Journal of Physical Chemistry A*, 2004, **108**, 5692–5698.
- 65 M. Ernzerhof and G. E. Scuseria, *The Journal of Chemical Physics*, 1999, **110**, 5029–5036.

- 66 R. Improta, V. Barone, K. N. Kudin and G. E. Scuseria, *Journal of the American Chemical Society*, 2001, **123**, 3311–3322.
- 67 R. Kaschner and D. Hohl, *The Journal of Physical Chemistry A*, 1998, **102**, 5111–5116.
- 68 V. Barone and C. Adamo, *The Journal of Chemical Physics*, 1996, **105**, 11007–11019.
- 69 F. Birch, *Phys. Rev.*, 1947, **71**, 809–824.
- 70 Y. Kuwayama, K. Hirose, N. Sata and Y. Ohishi, *Science*, 2005, **309**, 923–925.